Application of seismic attributes and post stack inversion to study different sand reservoir distribution, offshore Vietnam

Anh Thi Kieu Nguyen

Department of Geology, Faculty of Science, Chulalongkorn University, Bangkok, 10330, Thailand
Corresponding author e-mail: kieuanh.dvl54@gmail.com

Abstract

Nam Con Son Basin is one of the major hydrocarbon producing fields in offshore Vietnam. This field is characterized by complex tectonic settings with extensional activities and uplift events. The interest interval of the study area is the Post rift stage in Upper Miocene of Nam Con Son Basin which developed in a deep marine environment. Thus, the main sand reservoirs are recognized as turbidites with complex geometries which is challenging in understanding the reservoir properties based on conventional full stack seismic data. Goal of the study was to identify and predict the distribution of different sand reservoirs in Upper Miocene, using rock physics analysis and post stack inversion, in combination with seismic attribute analyses. Rock physics analysis greatly assists in the interpreted Post stack inversion by discriminating rock properties of different lithologies and fluids. RMS highlights amplitude anomalies correlated to coarser-grained sediments. Whereas, gas sand or stratigraphic features can be observed from high amplitude in low frequency using the attribute Spectral Decomposition. The gas bearing sand is low P-impedance while wet sand and shale show the higher P-impedance. As the results gained from these analyses, the distribution of different sand reservoirs were predicted based on the combination of Post Stack inversion and amplitude attributes. Furthermore, the special fluid (gas) bearing sand can be imaged by Spectral Decomposition and Post Stack inversion.

Keywords: Seismic attributes, Post stack inversion, Rock physics, Submarine fans, Sand geometries.

1. Introduction

The study area is located in the Northeast of Nam Con Son Basin (NCS) (Figure 1). The interest interval is in sediments of U5-formation mainly containing shale and siltstone interbedded with fine, whitish grey sandstone and thin layered carbonates. The main reservoirs range from continental deltas to deep marine turbidities (Liem, 2013). The distribution of turbidity sandstones has complex architectures and geometries due to the NCS tectonic setting. Therefore, it is critical to propose a workflow for the prediction of sandstone reservoir distribution. By using seismic interpretation and combining with well logging interpretation, and seismic attributes, especially Post-stack inversion, the opportunities of identifying sand bodies could be improved and reduced uncertainties which make the study more reliable than just using conventional seismic.

This thesis focuses on mapping the distribution of different sand reservoirs within the depth of interest interval based on conducting rock physics analysis, seismic attributes and post stack inversion.

2. Regional Geology

The NCS Basin is a rift basin which in its evolutional history is linked to the rifting and seafloor spreading that characterized the opening of the East Vietnam Sea (South China Sea). The main reservoirs of study interval were formed in post rift Stage-Upper Miocene.

The rifting period in the Eocene and into the Early Oligocene is controlled by N-S extension, associated with E-W oriented faulting and deposition of rift-fill sediments in local W-E trending sub-basin. The rifting phase in Eocene – Early Oligocene that was then followed by the spreading of East Vietnam seafloor, which propagated initially from E to W then WSW. At the end of Early Miocene, southwestward propagation of seafloor spreading continued by a continental breakup. This caused the second extension phase at the SW of the rift tip including NCS Basin that are associated with NE-SW normal faults and deposition of syn-extension sediments in NE-SW grabens. The second rifting phase was then followed by a thick post rift sequence (Upper Miocene - Pliocene - Quaternary) due to the increase in sediment supply with respect to onshore uplift and magmatism (Fyhn et al., 2009).

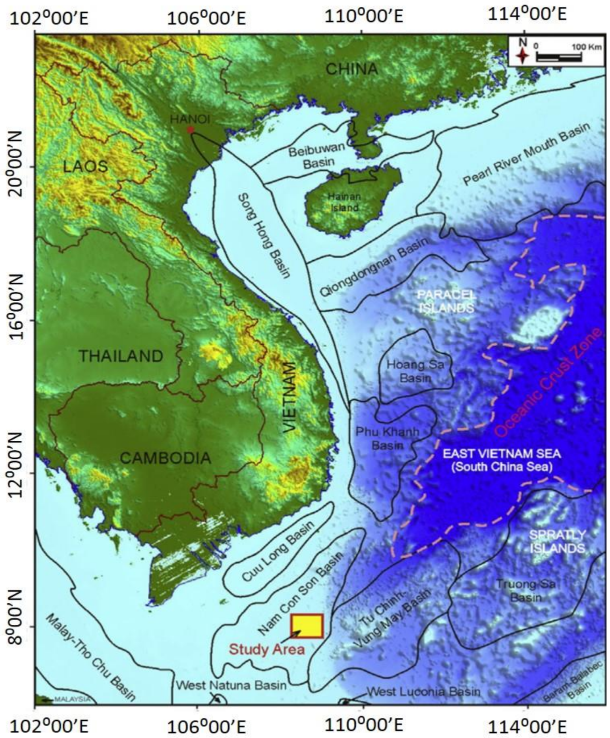

Figure 1: The location of the study area.

3. Database

The study area used approximately 656 km^2 of 3D seismic data, which starts from 0 to 4.5 seconds; Inline ranges from 1001 to 3105 and Crossline varies from 1821 to 4183. The bandwidth frequency ranges from 10 Hz to 40 Hz in window time between 2 and 3 seconds that contains sand reservoirs. Seismic data quality is quite good.

There are three deviated wells and final well reports used in the present study. The wireline log data includes Gamma Ray (GR), Density (RHOB), Sonic (DTC and DTS), Neutron and Resistivity. Moreover, the log curves vary in different depth ranges such as GR which has the largest length while other curves that focus on the reservoir intervals.

4. Methodology

4.1 Rock physics analysis

The aim of the rock physics analysis is to understand the fundamental behavior of key lithology and fluid combinations as a function of rock type, fluid content, reservoir quality and depth. The quantification of depth dependence is a key factor in the assessment of discriminators for lithology and fluid prediction purposes. The acoustic impedance (AI) is the result from multiplying density and P-wave velocity. The density and velocity against depth are colored by shale volume to help identify sand reservoirs in different depths. Moreover, cross plots of AI were plotted against gamma ray colored by water saturation to determine the rock physic parameters that distinguish lithology (sand, shale, and carbonate) and different fluids (gas sand and wet sand). Otherwise, cross plots of acoustic impedance versus shear velocity (Vs) for well KA-3 can help to separate wet sand and shale in the study interval.

4.2 Amplitude attributes and Post Stack Inversion

Root Mean Square (RMS) amplitude attribute: RMS calculates the square root of sum of squared amplitudes divided by the number of samples within the specified window used (Rotimi, 2014). It is applied to reveal bright spots and amplitude anomalies on the seismic data. The time window for RMS was selected depending upon the thickness of sands in this study area.

Spectral Decomposition (SD): Spectral decomposition of seismic data is a mathematical tool for transforming seismic data from time domain to frequency domain. High amplitude anomalies in low frequency zones are associated with the presence of hydrocarbon. It allows the localization of individual events in frequency space and enables the delineation of both the geometry and internal architecture of sediment transport system from seismic data (Castagna, 2003).

Post stack inversion: Seismic inversion is a technique that has been used to transform seismic data into AI, which is then used to make predictions about lithology and fluid distribution (Dubey, 2012). The post stack inversion was done using Hampson Russell software for full stack seismic data. There are three horizons including UMO, UMS1 and UMS2 applied for the model. Well KA-2 and KA-3 were used for controlling inversion results. Blind test well KA-1 was used for verifying the quality of matching between the inversion results and the well logs. The initial background model was created by using impedance logs of wells. P-impedance volume was computed using the initial low frequency model, a known wavelet and full stack seismic data. Model based inversion and colored inversion were built to determine which one is the most objective seismic inversion method to apply in the study area. The resulting acoustic impedance values from model based are heavily dependent on the interaction of the initial model. Whereas, colored inversion is only affected by the operator.

4.3 Depositional environment and sand geometries

The depositional environment was interpreted based on the cutting sample description, biostratigraphy from KA-1, electrofacies, seismic facies and seismic attributes. Moreover, the flow direction is enhanced by a consistent dip attribute. On the other hand, sand geometries were predicted from analyzing rock physics, attributes and inversion results.

*Consistent Dip***:** Consistent dip on the contrary uses an iterative global optimization method to calculate the dip in two different views (inline and crossline). A good dip estimation can reveal various structural geological features in seismic such as discontinuities (faults) and channels.

5. Result and interpretation

5.1 Rock physics analysis

Rock physics analysis was conducted for each well to detail information on rock properties. The lithology discrimination was based on the separation between sand and shale from the cutoff values of shale volumetric and gamma ray. Whereas, fluid indicator was determined by a cutoff water saturation. Following the cross plots below, sand was indicated by GR less than 90 API, Vsh <40% while gas sand responded to Sw ≤60% and water bearing sand was over 60 % of water saturation.

Lithology discrimination – The cross plots of Density, Velocity and P-Impedance versus Depth are shown in Figure 2

From the cross plots of Density, Velocity, Acoustic Impedance against Depth colored by Vsh for KA-1 in the depth interval 2500 to 3000 mBRT, UMS1 sand which is at the range from 2800m to 2900m has very low density from 2.1 g/cc to 2.2 g/cc compared to the higher density of shale at around 2.5 g/cc. Moreover, this sand is low P-impedance varying from 6000 to 6600 m/s*g/cc which is different from high P-impedance of shale in the range 7200-7800 m/s*g/cc. Some parts of sand UMS1 show the same impedance with shale due to the depth dependency. Therefore, different lithologies may have the same acoustic impedance within the larger interval.

On the other hand, there are two sands such as UMS1 and UMS2 found in KA-2 at the interval depth from 4700 to 5200m that are distinguished from shale due to low density ranging from 2.1 to 2.3 g/cc. P-wave of both sands show the same value with shale and in some parts illustrate very high P-wave because of carbonate cementation. In addition, sand UMS1 and sand UMS2 have the same range of acoustic impedance (7000 to 8500 m/s*g/cc) while acoustic impedance of shale ranges from 8500 to 9500 m/s*g/cc.

Sands in KA-3 could be distinguished from shale by density and P-wave. The sand in UMS1 reveals very low density of less than 2.24 g/cc. UMS2 sand has a higher density than UMS1 varying from 2.24 to 2.4 g/cc while shale shows very high density of approximately 2.55 g/cc. The velocity of UMS1 sand (3300 m/s) and UMS2 sand (3500 m/s) are slightly higher than shale (3000 m/s). Therefore, P-impedance of sand UMS1 (6800-7200 m/s*g/cc) is lower than shale which ranges from 7800 to 8500 m/s*g/cc. P-impedance of UMS2 sand (7000-8500 m/s*g/cc) indicates the same value with shale.

Fluid bearing indicators – The cross plot of P-impedance versus Gamma Ray and Shear velocity colored by Water Saturation is used as a fluid indicator.

To reduce the depth dependency in P-impedance, cross plot of AI, GR and Sw in KA-1 was plotted in the interval from 2800 to 2900 m. The UMS1 gas sand is confirmed by water saturation below 60 % and P-impedance ranges from 6000 to 7000 m/s*g/cc. The P-impedance of UMS1 gas sand is significantly lower than the P-impedance of shale which ranges from 7400 to 8400 m/s*g/cc (Figure 3).

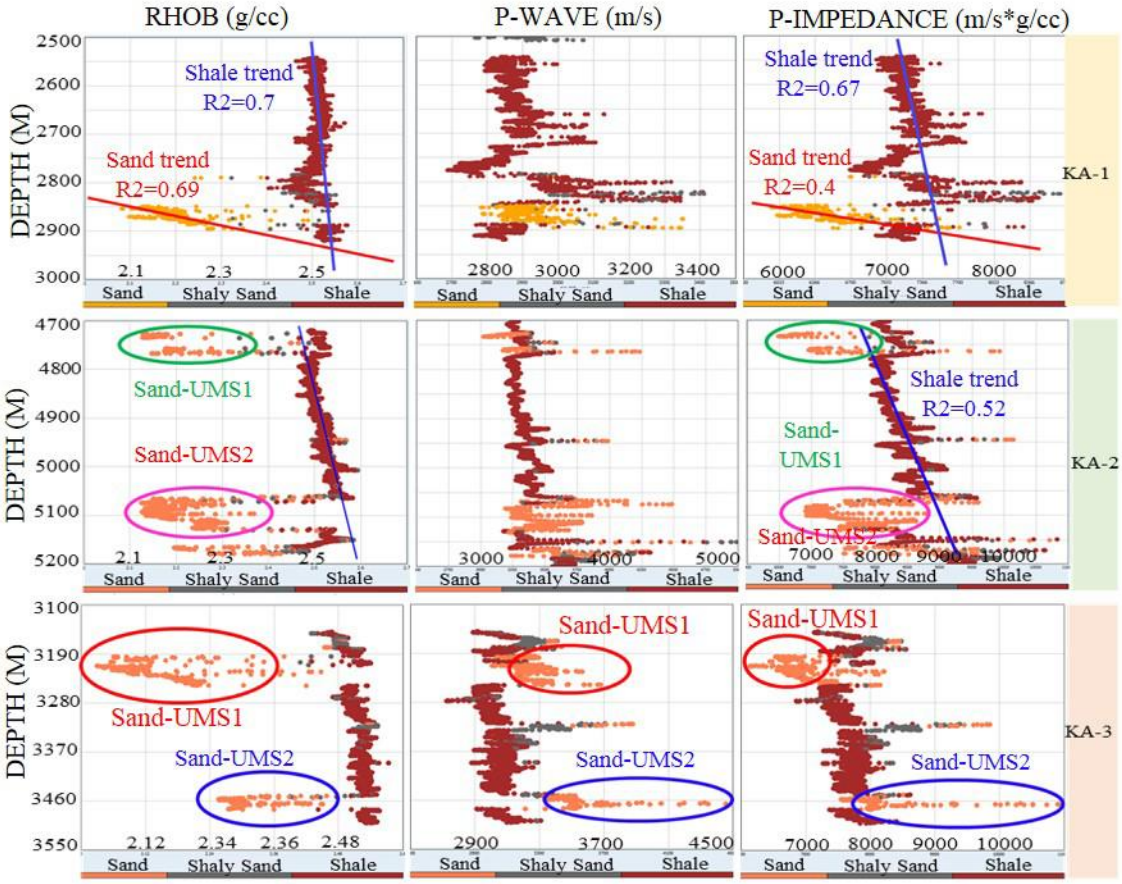

Figure 2: Sand and shale listed according to the measured depth could be distinguished by Density and Acoustic Impedance in three wells. P- Wave of sand and shale shows the same values in KA-1 and KA-2 while sands in KA-3 illustrates the higher velocity than shale.

The cross plot of gamma ray and P-impedance colored by water saturation for two different sands in the 100m interval at KA-2 shows that P-impedances of both UMS1 and UMS2 are much lower than shale. From Figure 4, the UMS1 sand shows AI varing from 6800 to 7800 m/s*g/cc. UMS1 contains two thin sands, the first sand (near Top UMS1) indicates a gas sand with low P-impedance (roughly 7000 m/s*g/cc). The second sand (near Base_UMS1) reveals a water bearing sand as the Sw reachs to 100%. The P-impedance of wet sand ranges from 7000 to 7800 m/s*g/cc. In contrast, UMS2 indicates a gas sand with P-Impedance from 6800 to 8200 m.s*g/cc. The shale impedance varies highly in interval of 8500 to 9500 m/s*g/cc. Some parts of UMS2 show the same P-impedance with shale due to cementaion effect.

In the well KA-3, the presence of a high percentage of gas within the depth interval 3100 to 3500 mBRT in UMS1 is shown as a decrease in P-Impedance of sand, which is significantly less than P-impedance of shale and wet sand. The P-impedance of UMS1 gas sand starts from 6500 m/s*g/cc while wet sand UMS1 varies from 7000-7500 m/s*g/cc. In comparison, wet sand UMS2 reveals a higher AI that averaged 8000m/s*g/cc. The acoustic impedance of wet sands is similar with the shale (7000-8500 m/s*g/cc) while P-impedance of carbonate cement is remarkably high with 10000 m/s*g/cc. Moreover, gas sand and wet sand show the separation with shale in the cross plot of P-impedance against shear velocity (Vs) colored by water saturation. Shear velocity of gas sand and wet sand are from 1750 m/s while shale reveals a lower value (1400-1700 m/s) (Figure 5).

According to the cross plots, sands can be distinguished from shale by density. Density of sand varies from 2.1 to 2.4 g/cc while shale is up to 2.6 g/cc. The P-impedance increases with the increase of shale content and gas occurrence reduces the acoustic impedance of sand. UMS1 gas sand shows a lower acoustic impedance than UMS2 gas sand. The P-impedance of UMS1 gas sand ranges from 6000-7200 m/s*g/cc while P-impedance of UMS2 gas sand varies in 7000-8200 m/s*g/cc. However, wet sand may have the similar P-impedance with shale.

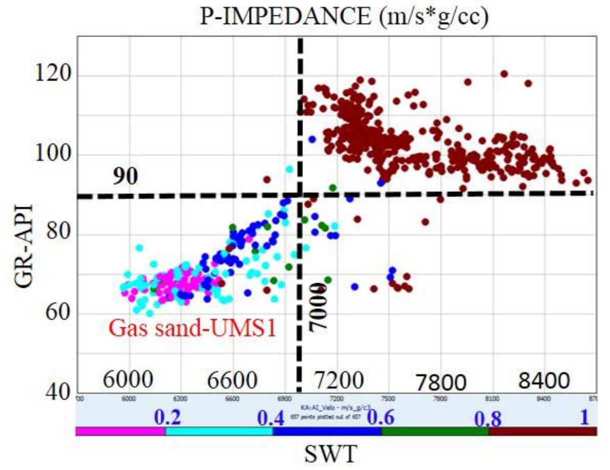

Figure 3: The cross plot of P-impedance against GR colored by Sw reveals that UMS1 gas sand corresponds to low GR, low P-impedance and below 0.6 water saturation in well KA-1.

Figure 4: Cross plots of AI, GR and Sw illustrate that gas sands indicate low AI, the P-impedance of UMS1wet sand is higher than UMS1 gas sand but is still lower than shale (top); the sand reservoirs are shown in vertical section (bottom).

Figure 5: The crossplot AI, GR and Sw reveals that gas sands reflect the low AI, wet sands show the same impedance with shale; Wet sand can be distinguished from shale by a higher Vs.

5.2 Amplitude attribute analyses

Root Mean Square (RMS) analysis

Gas sands correlate to very high amplitude RMS values (red) that were confirmed by wells. Wet sands in KA-2 (UMS1) or KA-3 (UMS2) are indicated by high RMS values (green to yellow). Whereas, low amplitude (dark blue) corresponds to shale domination that is consistent with Gamma Ray shown in KA-1 for UMS2. Hence, the high RMS amplitude (green to red) in this area could represent sand with different fluids distribution.

UMS2-RMS map reveals a narrow fan-shaped feature from amplitude anomalies. It starts with a canyon A' (800m wide) located in the Southwest and then spreads out to the N-NE (Figure 6 & 7). Whereas, UMS1-RMS shows the wider fan-shaped anomaly, located from SW to NE. The fan begins with two canyons A, B which are up to 1 km and 400 m wide respectively and extents outward to cover most the area.

Figure 6: RMS horizon slice of UMS2+30ms shows the fan-shaped feature due to the amplitude anomalies (left); A' & B' the indicator of channels in cross section.

Figure 7: RMS horizon slice of UMS2+30ms shows the fan-shaped feature due to the amplitude anomalies (left); A' & B' the indicators of channels in cross section.

Spectral decomposition

The gas reservoirs were observed at different low frequencies. At low frequency of 19 Hz, the significant high amplitude matched with gas sand at the well locations. In comparison with gas sands, wet sands in well KA-2 (UMS1) or KA-3 (UMS2) indicate lower amplitude (white to brown) while very low amplitude (dark blue) represents shale in well KA-1. Thus, high amplitude in low frequency spectral decomposition can provide useful information for identification of gas zone and sand distribution. From spectral decomposition maps of UMS2 and UMS1, fan-shaped feature can be observed clearly with amplitude anomalies (Figure 8).

Figure 8: The spectral decomposition maps of the UMS2+30 ms (a) and UMS1+30 ms (b) at 19Hz reveal the fan-shaped anomaly; gas sand (GS) corresponds to significant high amplitude, wet sand represents high amplitude while shale is low amplitude.

5.3 Post stack inversion

Initial model Building

Due to missing low frequency from seismic data, the initial model for post stack inversion was built by filtering P-impedance log data from 2000 ms to 4000 ms which covers the sand. In order to create the initial model, different low frequencies were tested for running inversion. As the inversion analysis results indicate, the low frequency 8-10 Hz was the most reasonable with the lowest error in the prediction of P-impedance at well locations.

Inversion analysis

The comparison of inverted pseudo logs (red) from P-impedance volume at the applied wells illustrates a close match with original P-impedance logs (blue) and follows the seismic trend, especially, with a good correlation at sand reservoirs indicating good inversion results. The Error ranges from 274.75 at KA-3 to 360 for KA-2. Whereas, pseudo log (7100 m/s*g/cc) of the blind test well KA-1 is slightly higher P-impedance than original log (6700 m/s*g/cc) at UMS1 sand reservoir. The error is roughly 572. However, pseudo log still follows the trend of the original log which represents the significant differentiation between gas sand and shale. Hence, the result of inversion process is reliable (Figure 9).

Figure 9: The inversion analysis for applied wells KA-2 and KA-3 shows the good match between original log (blue) and inverted log (red); the blind test well KA-1 reflects the slight separation between these logs. However, inverted log still follows the trend indicating gas sand and shale from original log.

Comparison of seismic inversion result and original logs

The result of post stack inversion was cross-checked with three wells in which KA-2 and KA-3 were used to build the inversion model. Well KA-1 is the blind test well for each surface. In general, there is good agreement between original logs and the P-impedance derived from the inversion volume in the interest zone. The P-impedance horizon slice was generated along horizon Top UMS2 in a 10ms window. The red to yellow indicates low impedance while the dark blue represents high P-impedance. Throughout the inverted cross section, KA-2 proved the gas sand with low P-impedance which matches with inverted P-impedance of seismic volume. Wet sand in well KA-3 and a part of KA-2 reflects high P-impedance from inverted volume as well as the original logs. The blind test well KA-1 is dark blue reflecting shale which is consistent with GR that shown shale in the section (Figure 10).

Following the P-impedance horizon slice conducted along horizon Top UMS1 in the 20ms window (Figure 11), sand UMS1 in KA-3 and the first thin sand in KA-2 proved the highly gas saturation sand with low acoustic impedance illustrates a significant fit with the inverted volume. Whereas, wet sand in KA-2 also indicates the high P-impedance in both inverted volume and original logs. The blind test well KA-1 is analyzed as full gas saturation with low P-impedance that is matched with the inversion result.

Figure 10: The result of Post stack inversion in UMS2 is equivalent to the wells as low P-impedance (red) corresponds to gas sand in KA-2 and Wet sand in KA-3; shale in KA-1 reflects high P-impedance (blue).

Figure 11: The result of post stack inversion in UMS1 is equivalent with the wells as low P-impedance (red) indicates for gas sand in KA-3, KA-1 and the first sand in KA-2; high impedance illustrates for wet sand in KA-2.

5.4 Depositional Environment

Depositional environment was interpreted based on cutting sample description, biostratigraphy analysis (well KA-1), seismic facies and seismic attributes.

The cutting sample description has a predominance of mudstones in most of the wells. The biostratigraphy analysis (deep water

Foraminiferal as *Cyclammina* spp., *Eggerella* spp.,) in well KA-1 suggest the widespread development of deep marine facies. In addition, seismic attributes such as RMS or Spectral Decomposition maps of both UMS1 and UMS2 provide the images of submarine fan formed by gravity flows in the deep sea environment. The submarine fans originated from SW and then spread out to N and NE by submarine canyons (Figure 6&7). From the entry point toward the E, there are sub-linear features on the consistent dip maps (Figure 12) which may represent flow directions. In the map for UMS2 sand shown in Figure 12, a channel can be seen clearly with sinuous shape trending across the map and stopping at the fault. This can be the main reason for not encountering UMS2 sand in well KA-1 because the channel controlled sand distribution.

On the other hand, seismic facies of both UMS1 and UMS2 reveal semi-parallel and continuous reflection along the fan-shaped high amplitude areas that are indicating turbidites (Figure 13). The results are consistent with observations on GR responses which have stacking patterns of blocky shape with sharp top and base (Figure 4 & 5).

Figure 12: Consistent dip on time slice Z=2620 ms–UMS2 (top) and Z=2450 ms-UMS1 (bottom) reveals some channels, faults and flow directions.

Figure 13: Semi-parallel and continuous reflection on the cross section along the high amplitude area of UMS2 (a) and UMS1 (b).

Figure 14: The schematic of depositional environment with reference in the study interval (Dung et al., 2018).

5.5 Sand distribution by integrating seismic attributes and seismic inversion

Gas sand distribution

By applying cut-off values observed in rock physic analysis, the gas sand intervals can be imaged on the inverted P-impedance section. Gas sand shows significant low impedance (7000-8200 m/s *g/cc for UMS2 and 6000-7200 m/s*g/cc for UMS1) in the horizon slices. Whereas, significantly high amplitude in low frequency from spectral decomposition corresponds for gas sand. Therefore, the spectral decomposition along with P-impedance inversion can be useful for hydrocarbon prediction.

From the extracted P-impedance horizon slice of UMS2 in the 10ms window, there are three boundaries which are interpreted as gas distribution from the cut off value. However, two gas sand geometries interpreted on spectral decomposition are consistent with inversion results. As a result, on the combination SD+RMS map, the gas sand UM2 distributes at two locations. The first is located around the well KA-2 and another is located 2km away to the northern of well KA-2 (Figure 15).

On the other hand, gas sand UMS1 is interpreted on the horst closured at main faults and submarine channels located in the NE of the study area as the extracted P-impedance horizon slice UMS1+20ms show. These interpretations are consistent with the result of spectral decomposition (Figure 15).

Figure 15: The distribution of gas bearing sand by combining the results of inversion and SD 19Hz of UMS2 (top) and UMS1 (bottom).

Sand distribution

The P-impedance of UMS1 wet sand (7000-7500 m/s*g/cc) and UMS2 wet sand (7500-8000 m/s*g/cc) overlap with the P-impedance of shale. Therefore, it is not easy to discriminate sand and shale zones in this interval. However, sands are characterized by high amplitude while shale is low amplitude. This statement is proven by RMS and SD analyses. Hence, combining post stack inversion with amplitude attributes may be useful for predicting the sand distributions.

The geometry of UMS2 sand was interpreted based on amplitude anomalies and cutoff P-impedance of sand (7800 m/s*g/cc). From RMS horizon slice (Figure 16), the sand distribution was interpreted following a fan-shaped area. This is equivalent with the result of spectral decomposition (SD) horizon slice. Moreover, RMS cutoff of 70 for sand overlying with SD suggests that the high amplitude of RMS is consistent with the anomaly amplitudes of spectral decomposition. Inversion results indicate sand dominating in the NNE. From these results, UMS2 sand has a NNE-SSW orientation. The sand spreads out widely in the NNE and pinches-out in the SSW. In addition, three local sands were observed. The first channel-fill is oriented NW-SE playing as a sediment point source to transport the sand. The others are located in the South of the study area (Figure 16).

The sand UMS1 was predicted from analyzing high amplitude of Spectral decomposition at 19 Hz and RMS map. From SD+RMS horizon slice (Figure 17), the sand distribution follows the trend of high amplitude RMS cutoff value of 90 which is equivalent to the amplitude anomalies of SD in the background. The horizon slice from inverted volume illustrates the sand (cutoff 7500 m/s*g/cc of P-impedance) dominating at the center and developing to the NE. Consequently, UMS1 sand represents a widespread fan in this study area. The major distribution of sand is on the structural high and spreading to the NE. This sand pinches-out to the North and the West. The amount of clean sand could be reduced to the East. There are three channel fills. The first one has the SW-NE trend which acted as the main sediment point from the submarine fans. The others are in the Southern direction (Figure 17).

Figure 16: The sand distribution was identified based on amplitude anomalies from SD, RMS and inversion results. UMS2 sand spread outs to the NNE and pinch-outs to the SSW.

Figure 17: The sand distribution was identified based on amplitude anomalies from SD, RMS and inversion results. UMS1 sand represents a widespread fan in the study area. It develops to the NE and pinches-out to the N and W.

6. Discussion

6.1 Depositional environment and tectonic setting control of sand distribution

There are two main factors controlling the sand distribution including depositional environment and tectonic settings although other factors such as slope dip, sediment supply and bathymetry can also play important roles as well. A large amount of sediments can reach slope and basinal regions along with a significant fall of sea level. In this context, strong erosion occurs in the onshore basin drainage forming incised valleys in environments of near-shore and shelf. In the offshore slope region, development of sub-marine canyons will facilitate transportation of sediments beyond the slope and deposition on the basin floor. At the distal ends of canyons, the turbidity currents spread out to form a lobe of turbidite deposits that occupies a portion of the fan surface. For UMS2, there are two identified sediment entry points from the shelf located to the West. One sediment entry point was located in the SW and the other one was from the horst of study area. Whereas, UMS1 has the sediment point sources from the main submarine canyon located in SW of the study area. Since fine-grained sands are dominant and the wells are located far from the source points in UMS1, the sand was likely to be deposited in a more active depositional area. In contrast, UMS2 is believed to be near slope deposits with dominant coarse-grained sandstone found in KA-2 and KA-3. The absence of this sand in KA-1 indicates the limitation in the distribution when it comes to a more proximal part of the fan (Figure 18).

The development of normal fault system created the accommodation space for the deposition of sediments. The sediments from the platform followed the canyons (consistent dip Figure 12) and flow directions to fill the hanging wall of the fault. The effects of tectonic activities can be observed clearly by the different geometries in sands. The sand distribution of UMS2 which is present in well KA-2 follows channels oriented by faults.

Figure 18: The location of two sands on submarine fans. UMS2 is located nearby a slope while UMS1 distributes in the more active depositional area of fan.

6.2 Limitations of seismic data

UMS1 includes two sands (4m and 6m thickness) which reflect the different strong amplitude in synthetic seismogram, but these sands display one relatively strong amplitude in seismic traces due to the low resolution of seismic compared to well log (Figure 19). The tuning thickness of 29m for the UMS1 was calculated by using 20Hz dominant frequency and the velocity from well KA-2. Hence, the interpretation of thin sands cannot be separated on the conventional seismic. It means that the gas bearing sand in UMS1 may not be accurate for the area that contains sands below the resolution of seismic. The amplitude attributes such as RMS and SD are not effective to separate these sand. However, post stack inversion helps to reduce the effect of wavelet that enhances the resolution of P-impedance cube.

The post stack inversion cannot distinguish wet sand and shale in the study area. Using the P-impedance cutoff for sands may contain shale and the sand distribution results have some uncertainties. However, wet sand may be recognized by very high shear velocity compared with shale (Figure 19). Hence, simultaneous inversion or AVO may be more appropriate for prediction of different fluids and sand distribution.

Figure 19: a- Thin sands cannot be distinguished on the seismic trace; b- wet sand may be recognized by high Vs from the cross plot P-impedance, Vs and Sw.

7. Conclusion

The prediction of different sand geometries was conducted effectively by integrating the results of rock physic analysis, combination of seismic attributes and post stack inversion.

Rock physics parameter including density, P-wave, P-impedance and shale volume revealed that acoustic impedance depends on depth and lithology can be discriminated at study interval. Water saturation, P impedance and Gamma ray are used to identify the fluids in the reservoir. The presence of gas accumulation responds to low Acoustic impedance while wet sand and shale show the same P-impedance.

High amplitude anomalies of RMS and Spectral Decomposition (SD) indicate coarser-grains as well as sand reservoir. Post stack inversion cannot distinguish completely between sand and shale. However, integrating Post Stack inversion and amplitude attribute can be useful for predicting the sand distribution. Especially, gas sand is highlighted by very high amplitude in SD and low P-impedance. Thus, combining SD and Post stack inversion help to interpret gas sand geometries.

8. Acknowledgement

I sincerely thank PetroVietnam – Vietnam oil and Gas Group (PVN) for their financial support and for giving me the excellent opportunity to study in the Petroleum Geoscience Program as well as Vietnam Petroleum Institute and Exploration & Production Centre.

I also would like to express my deepest gratitude to my supervisor: Professor Angus John Ferguson, the principal adviser of my project, for giving so generously of his time. Specially, thanks to all the lecturer and staffs for their teaching and helping during the year.

9. Reference

Castagna O., Instantaneous spectral analysis: Detection of low-frequency shadows associated with hydrocarbons. The Leading Edge (2003): 120-127.

Dubey, A. K. Reservoir characterization using AVO and seismic inversion techniques. Journal of Society of Petroleum Geophysicists (2012): 1-7.

Dung, B.V., Tung, N.T., Kieu, N.V., Huyen, N.T.D., Tuan, H.A., Giang, K.H. Depositional facies and environments of Oligocene- Miocene sediments in the central part of Nam Con Son Basin, Southeast Vietnam Shelf. Journal of ELSEVIER (May, 2018): 1-10.

Fyhn, M.B.W, Boldreel, L.O., and Nielsen, L.H. Geological development of the central and South Vietnamese margin: implications for the establishment of the South China Sea, Indochinese escape tectonics and Cenozoic volcanism. Tectonophysics (2009): 184-204.

Liem, P.T., 2013. Some comments on the possibility of middle/ late Miocene – Pliocene stratigraphic traps in the center of Nam Con Son basin. Journal of PetroVietnam Vol.10 (2013).

Pigott, J.D., Kang, M.H., and Han. First order seismic attributes for clastic seismic facies interpretation: Examples from the East China Sea. Journal of Asian Earth Science Vol. 66 (2013): 34-35.

Rotimi, O.J., Wang, Z., Ako, D.B. Seismic attribute utilization for structural pattern detection, fault imaging and prospect identification. Journal of Petroleum & Coal (2014): 532-543.